Modeling Hydrodynamics of Trickle-Bed Reactors at High Pressure

C. S. L. Narasimhan and R. P. Verma
Research & Development Center, Indian Oil Corporation Limited, Sector-13, Faridabad-121007, India

Arunabha Kundu and K. D. P. Nigam
Dept. of Chemical Engineering, Indian Institute of Technology, Delhi Hauz Khas, New Delhi-110016, India

A phenomenological hydrodynamic model of a trickle-bed reactor developed predicts pressure gradient and liquid holdup at high pressures. The model consists of 1-D force balance equations incorporating particle–gas drag, particle–liquid drag and gas–liquid interactions. The deviation between the measured and theoretical pressure drop is explained in terms of tortuosity and axial dispersion effects. Tortuosity encountered by the flowing liquid and gas phases has two components: (1) tortuosity angle (θ), the measure of the tortuous path the fluid would take; (2) an excess friction factor, which would approximate for resulting excess drag while the tortuous path is taken. These parameters were observed to play a major role in modeling the hydrodynamics in the trickle-bed reactor. The model takes into account the tortousity effects in a unique way. The axial dispersion effect comes into the picture due to the back-mixing, modeled in terms of the Peclet number (Pe) in a novel way. The overall model was tested with major experimental data for the high-pressure concerning various types of gas–liquid systems, including hydrocarbons, aqueous solutions, coalescence inhibiting liquids, and so on, that are available in the literature, and the prediction has been found to be excellent.

Introduction

Trickle-bed reactors are three-phase catalytic randomly packed fixed-bed tubular reactors in which liquid and gas phases flow cocurrently downward or countercurrently. The majority of processes occurring in commercial trickle-bed reactors are performed at elevated pressure of about 2–30 MPa in order to slow down catalyst deactivation, improve the solubility of gaseous reactant, attain high conversion and achieve better heat transfer. Recently, some reviews on the state-of-the-art trickle-bed reactor hydrodynamics have appeared (Saroha and Nigam, 1996; Iliuta et al., 1999).

Pressure gradient and liquid holdup

A fundamental understanding of the hydrodynamics of trickle-bed reactors is necessary in their design, scale-up, and performance. The hydrodynamics are affected differently in each flow regime (Charpentier and Favier, 1975; Specchia and Baldi, 1977; Rao and Drinkenburg, 1985; Kundu et al., 2001). Of particular interest in the industry is the extensively used trickle flow encountered at low gas and liquid superficial velocities. The basic hydrodynamic parameters are the pressure gradient and liquid holdup.

Two-phase pressure gradient is defined as the variation of the internal pressure per unit-reactor length. The pressure gradient is related to the mechanical energy dissipation due to the two-phase flow through the fixed bed of solid particles. It is important in evaluating the mechanical energy losses, in sizing equipment for pumping and compression of the fluid (Tosun, 1984), and it is used in correlating gas–liquid and liquid–solid mass transfer (Gianetto et al., 1973).

Liquid holdup (h_L) is defined as the volume of liquid contained in the bed per unit-bed volume. It is a function of physical properties of the fluid phases and the bed character-

Correspondence concerning this article should be addressed to R. P. Verma and K. D. P. Nigam.

istics. It is a basic parameter for reactor design, because it is related to other important parameters, namely, pressure gradient, gas–liquid interfacial area, the mean residence time of the liquid phase, catalyst loading per unit volume, axial dispersion coefficient, and mass-transfer and heat-transfer coefficients. The term total liquid saturation (β_t) is used to describe the amount of liquid in the bed and is defined as the volume of liquid present in a unit void volume of the reactor. Thus, the liquid holdup and total liquid saturation are given as

$$h_L = \epsilon\beta_t. \tag{1}$$

If the catalyst particles are porous, the total liquid saturation (β_t) is the sum of internal or intraparticle liquid saturation and the interparticle or external liquid saturation. The external liquid saturation is further divided into residual or static liquid saturation (β_s) and free-draining or dynamic saturation (β_d). The static liquid saturation is a function of the physical properties of the liquid and particle shape, size, and wettability. The dynamic liquid saturation is the fraction of liquid volume collected on draining the reactor after simultaneously closing the inlet and outlet streams. It depends on liquid and gas flow rates, the physical properties of the fluid and packing characteristics. The dynamic liquid saturation can be considered to be the volume of liquid in the reactor, which is continuously being renewed, while static liquid saturation can be considered to be the volume of liquid held on the surface of the particles, at the contact points between the particles and the wall, which remains stagnant. There are three different techniques—tracer, drainage, and weighing—for the measurement of liquid holdup in a laboratory trickle-bed reactor operating at high pressure. Among these three methods, tracer and drainage techniques give comparable values for the total liquid holdup (Al-Dahhan and Highfill, 1999; Nigam et al., 2001; Pant et al., 2001).

There have been mainly two different approaches to modeling trickle-bed hydrodynamics reported in the literature. The first and the classic one is the empirical approach, which is widely reported for low-pressure systems. These approaches have very low-range predictability and are most of the time specific to a particular liquid and gas system. Recently, correlations for high-pressure operations have been reported where it has been found that regime transitions and flow behavior vary with an increase in pressure. The boundary line between the trickle-flow regime and pulsing-flow regime shifts toward higher gas throughputs for a given liquid flow rate with the increase in pressure. Another recently developed approach is to describe hydrodynamics in a phenomenological manner, which is semitheoretical in nature and based on the physics of the process. Although these approaches have a wider range of predictability, some of them still use certain correlations that limit their range of predictability. Most models in this category predict the data within a confidence limit of $\pm 40\%$.

The main objective of this work is to develop a unified approach of modeling the hydrodynamics of trickle-bed reactor based on fundamental force balances with low empiricism, which is valid for a wide range of operating pressures. The model has capabilities of predicting pressure drop and liquid holdup at different operating conditions. The model predictions have been found to be in agreement with almost all prominently published data on hydrodynamics within an average confidence limit of $\pm 14\%$.

Literature Review

Pressure gradient and liquid holdup

A large number of studies have been reported in the literature on various hydrodynamic aspects of trickle-bed reactors. Several correlations and models of pressure gradient and liquid holdup have been developed from these studies. The correlations and models based on the atmospheric data are summarized in the articles of Charpentier et al. (1969), Sai and Varma (1987), Ellman et al. (1988, 1990), Holub et al. (1993), and Saroha and Nigam (1996). Investigations on high-pressure trickle-bed reactors have been carried out by Hasseni et al. (1987), Ellman et al. (1988, 1990), Wammes and Westerterp (1991), Wammes et al. (1991a,b), Larachi et al. (1991a,b), and Al-Dahhan and Dudukovic (1994). These studies have shown that the hydrodynamic parameters are greatly affected by gas density, and the correlations and models based on data at atmospheric pressure are not valid in the whole range of operating pressure.

The existing hydrodynamic models can be broadly classified into two different categories. The first category uses an empirical approach based on dimensional analysis to produce explicit correlations for pressure drop and holdup (Larkins et al., 1961; Turpin and Hungtinton, 1967; Sato et al., 1973; Midoux et al., 1976; Clements and Schmidt, 1980; Sai and Varma, 1987; Ellman et al., 1988, 1990; Larachi et al., 1991a,b; Wammes et al., 1991a,b; Xiao et al., 2000). These correlations have several parameters for fitting the experimental results. These parameters are not universal constants. The predicted values of pressure gradient and liquid saturation from these correlations vary considerably. The second category involves the development of models resulting from equations of motion and considers determination of drag forces of gas and liquid phases at various operating regimes. Four distinct approaches have been used in this category: (1) the relative permeability model, (2) fundamental force balance model, (3) the slit model, (4) the 1-D CFD model. In the relative permeability concept, the Ergun (1952) equation (which is basically for single-phase flow and arises from a momentum balance in an assumed pore geometry) has been modified to account for the existence of a second flowing phase. The relative permeability of each phase has been correlated as a function of the liquid saturation of each phase, depending on the experimental results (Sweeney, 1967; Specchia and Baldi, 1977; Sáez and Carbonell, 1985). The fundamental force balance model developed by Tung and Dhir (1988) involves force balance equations in liquid and gas phase in an elemental reactor volume. In their work, modeling has been done using the cocurrent upflow and countercurrent mode of operation rather than the conventional downflow mode. The phenomenological slit model developed by Holub et al. (1992, 1993), Al-Dahhan and Dudukovic (1994), and Iliuta et al. (2000) involves point equations of flow for each phase in the pore scale, and use volume averaging to establish a bed scale model. Initially, Holub et al. (1992, 1993) modeled the complex geometry of the actual void space in the catalyst bed at the pore level by correlating it with the phenomenon of flow

inside a rectangular slit. In their model, the width of the slit is a function of bed porosity, and the angle of inclination of the slit to the vertical axis is related to a tortuosity factor for the packed bed. They introduced the concept of slip of the velocity and shear at the gas–liquid interface by introducing two slip parameters. The resulting pressure-drop and liquid-saturation model of Holub et al. indicates zero shear stress at the gas-liquid interface. This result implies that the gas flow does not influence the liquid flow. Al-Dahhan and Dudukovic (1994) attempted to validate the phenomenological model of Holub et al. (1992) based on their experimental data on the pressure gradient and liquid holdup obtained in an operating pressure range of about 0.31–5 MPa, and found that it did not fit well with the data in the high-interaction and high-pressure regimes. Later, Al-Dahhan et al. (1998) obtained the correlations for the slip parameters as a function of gas- and liquid-phase Reynolds numbers to fit high-pressure data. Holub et al. (1992, 1993) and Sáez and Carbonell (1985) assumed that the phase interaction terms are negligible, though, in reality, weak interfacial gas–liquid interaction prevails only at very low superficial gas and liquid velocities. Iliuta et al. (2000) developed the double-slit model, which considers the distribution of totally dry slits in addition to the wet slits, as in Holub et al. (1992, 1993). They used the same slip factors that Al-Dahhan et al. (1998) used. Recently, Attou et al. (1999) developed a model based on macroscopic mass- and momentum-conservation laws, in which the drag force has a contribution to both particle–liquid and gas–liquid interactions. Since these models are based on the fundamental approach and contain mechanistic details of the system, they have a wider range of applicability unlike the correlative models, which are system specific. The present trend is to develop models based on the fundamental approach to exploit their wider range of applicability. Different approaches for modeling trickle-bed reactor hydrodynamics have been discussed in detail by Saroha and Nigam (1996).

The present article attempts a physics-based approach in order to model pressure drop and liquid holdup at high-pressure operation of the trickle-bed reactor. The study focuses on the basic approach of fundamental force balance with modification for the downflow mode to present a more realistic picture of the complex hydrodynamics prevailing in the reactor. Variations in the tortuous path and tortuosity effects with flow parameters have been determined to be of prime importance. The phenomenological analysis of Holub et al. (1992, 1993) has been used as an appropriate starting point in proposing a novel model for this effect. The result is thus a unified approach in modeling of the hydrodynamics of a trickle-bed reactor.

Model Development

Liquid- and gas-phase force balance

In an attempt to depict the physics of the process as accurately as possible, point force balances were applied to the two flowing phases. Gas- and liquid-flow configurations in a unit-volume cell representing cross-sectional averaged flow conditions are shown in Figure 1. The annular configuration has been postulated here, but such a force balance should be equally applicable to other flow regimes, provided the effect of flow regimes is determined elsewhere.

Gas-Phase Force Balance. Since particles are not in direct contact with the gas, their effect on the gas phase is strictly restricted to what is felt across the liquid layer. Therefore, the interfacial drag between the two flowing phases is broken into two components, as shown in Figure 2. The first component, F_{PG}, is opposed by an equal and opposite force applied by the particles on the other side of the liquid layer. In this context, F_{PG} can be viewed as a particle–gas drag. The second component, F_I is the drag force on the gas caused by the relative motion between the two phases. Thus if α is the gas saturation and β is the liquid saturation, the force balance

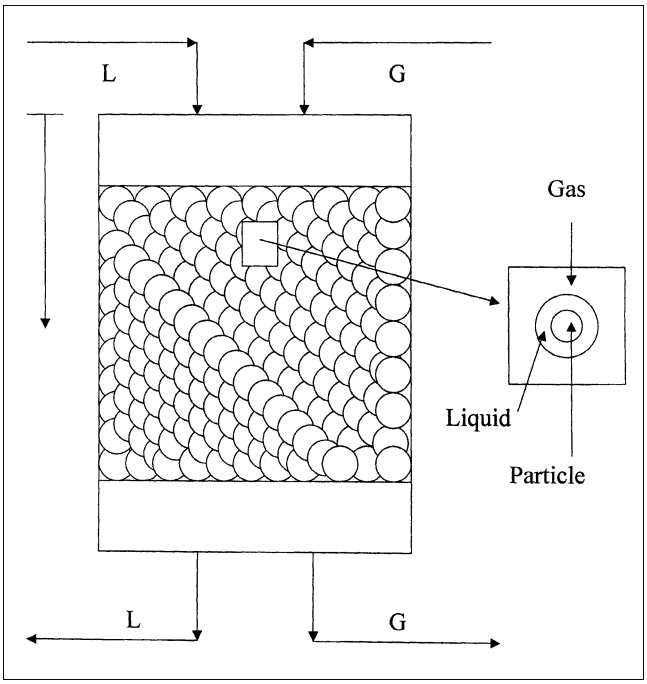

Figure 1. Two-phase flow in a unit-volume cell in a trickle-bed reactor.

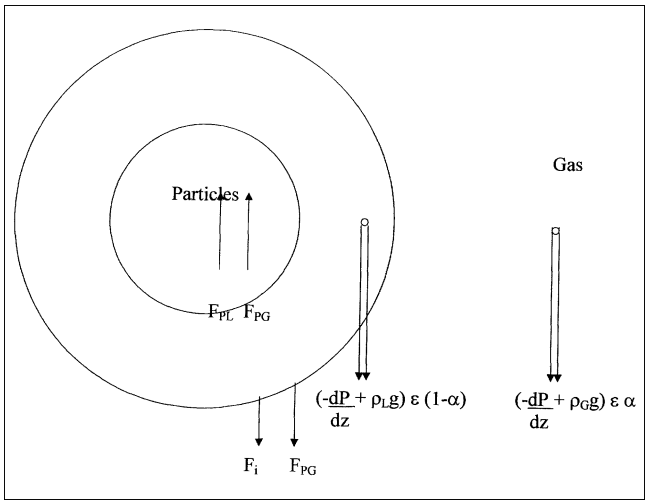

Figure 2. Different drag forces while two-phase flows over catalyst particles in a trickle-bed reactor.

on the gas phase is given by

$$\left\{-\frac{dP}{dz}+\rho_G g\tau\right\}\alpha\epsilon = F_{PG}+F_I. \tag{2}$$

Liquid-Phase Force Balance. Similarly, the liquid-phase force can be split into two components, F_{PG} and F_{PL}. The first component, F_{GP}, is simply a reaction to the force by which the gas pushes the liquid against the particles. The second component, F_{PL}, represents the force acting on the particles due to the liquid motion. The force balance on the liquid then yields

$$\left\{-\frac{dP}{dz}+\rho_L g\tau\right\}(1-\alpha)\epsilon = F_{PL}-F_I. \tag{3}$$

It should be noted that F_{PG}, F_{PL}, and F_I represent the drag forces per unit of total bed volume. Since the size of the particles considered in this work is large, the capillary effect will be confined to a very small fraction of the pore volume, and hence is neglected. Because of the interfacial tension, the pressure in the gas phase will be slightly higher than in the liquid. However, the pressure difference between gas and liquid will remain constant in the direction of flow. As such, the pressure gradient in the direction of flow is the same for both phases. By defining the dimensionless variables

$$P^* = \frac{-\dfrac{dp}{dz}}{g(\rho_L-\rho_G)} \tag{4}$$

and

$$\rho^* = \frac{\rho_G}{\rho_L} \tag{5}$$

$$F^* = \frac{F}{g\epsilon(\rho_L-\rho_G)}, \tag{6}$$

Eqs. 2 and 3 become

$$P^*\alpha = -\frac{\rho^*\alpha\tau}{(1-\rho^*)}+F^*_{PG}+F^*_I \tag{7}$$

and

$$P^*(1-\alpha) = -\frac{(1-\alpha)\tau}{(1-\rho^*)}+F^*_{PL}-F^*_I. \tag{8}$$

Equations 7 and 8 involve five variables, and so three more relationships are needed before these equations can be solved explicitly. Thus, models for the three variables, F_{PG}, F_{PL}, and F_I, are first proposed before proceeding any further.

Modeling of the drag forces

Particle–Gas Drag Model. The particle–gas drag force is obtained using the Ergun equation (McCabe et al., 1993). Since the liquid is always in contact with the particles and F_{PG} is being modeled as the force by which the gas pushes the liquid against the particles, the system of particles and liquid can be considered as an isotropic layer with porosity $\epsilon\alpha$. Also, the particle diameter must be corrected for the increase in particle volume due to the liquid layer, yielding an effective diameter of $[(1-\epsilon\alpha)/(1-\epsilon)]^{1/3}D_P$. Using these corrections, the expression for dimensionless particle–gas drag is given by

$$F_{PG} = \frac{a^*\mu_G V_G}{\kappa_G}+\frac{b^*\rho_G V_G^2}{\eta_G}, \tag{9}$$

where

$$a^* = \frac{a}{g(\rho_L-\rho_G)}, \qquad b^* = \frac{b}{g(\rho_L-\rho_G)}, \tag{10}$$

and

$$a = 150\frac{(1-\epsilon)^2}{\epsilon^3 D_P^2}, \qquad b = 1.75\frac{(1-\epsilon)}{\epsilon^3 D_P}, \tag{11}$$

and κ_G and η_G are relative permeabilities, which depend on the flow regime. The relative permeabilities are defined as

$$\kappa_G = \left(\frac{1-\epsilon}{1-\epsilon\alpha}\right)^{4/3}\alpha^2 \qquad \text{and} \qquad \eta_G = \left(\frac{1-\epsilon}{1-\epsilon\alpha}\right)^{2/3}\alpha^2. \tag{12}$$

Particle–Liquid Drag Model. The particle–liquid drag can be modeled in the same manner as the particle–gas drag. However, since the liquid is always in contact with the particles, the particle diameter and the solid fraction term $(1-\epsilon)$ in parameters a and b need not be corrected. Nevertheless, porosity should be multiplied by $(1-\alpha)$. Also, the liquid follows a tortuous path even up to $\alpha \sim 1$ and all of pore space is accessible to it. As such, the liquid-friction pressure drop will be similar to that for the gas. The dimensionless particle–liquid drag is thus given by

$$F^*_{PL} = \frac{a^*\mu_L V_L}{\kappa_L}+\frac{b^*\rho_L V_L^2}{\eta_L}, \tag{13}$$

where

$$\kappa_L = \eta_L = (1-\alpha)^3. \tag{14}$$

Liquid–Gas Interfacial Drag Model. The interfacial drag, F_I, is defined as the total drag on the gas phase per unit volume of the porous layer induced by the relative motion between the two phases. The approach that has been used is to first develop an expression for the drag on a single bubble/slug and then multiply it by the number of bubbles/slugs per unit volume of the porous layer. The dimensionless form

of the interfacial drag is obtained as

$$F_I^* = C'_V \frac{V_L V_s}{gD_b^2(1-\rho^*)\epsilon} + C'_I \frac{(1-\alpha+\rho^*\alpha)V_s}{gD_b(1-\rho^*)\epsilon^2}, \quad (15)$$

where V_s is the drift velocity of the bubble relative to the mixture, given by

$$V_s = V_G \frac{(1-\alpha)}{\alpha} - V_L. \quad (16)$$

The coefficients C'_V and C'_I depend on the flow regime prevailing. A detailed derivation of these, along with the mathematical modeling of the flow regimes is given in Tung and Dhir (1988).

Model for Tortuosity Effect. The tortuosity effect has to account for the excess drag that occurs due to the different tortuous paths followed by the streams at different velocities. The first aspect accounts for relative reduction in buoyancy force due to the excess twisted distance traveled by the fluid element, and the second effect is momentum lost by the fluid element in doing so. In order to account for these aspects and obtain a realistic estimate of tortuosity, a force balance has been visualized on an element of fluid mass moving along an inclined plane. This is shown in Figure 3. Because the gas and liquid actually traverse a tortuous path, which is physically difficult to depict, the entire effect of tortuosity is lumped into the inclined plane effect.

The tortuosity, as just depicted, corrects the gravity term of Eqs. 7 and 8. The gravity effect in the force balance of liquid and gas phases is thus observed as $(g \cos \theta - \mu g \sin \theta)$, where θ accounts for the distance traveled in the tortuous path, and μ accounts for the excess loss in force due to drags on the liquid and gas following the tortuous path. Also, θ and μ are actually functions of the superficial liquid and gas velocities. Thus, with this approach, the term $(\cos \theta - \mu \sin \theta)$

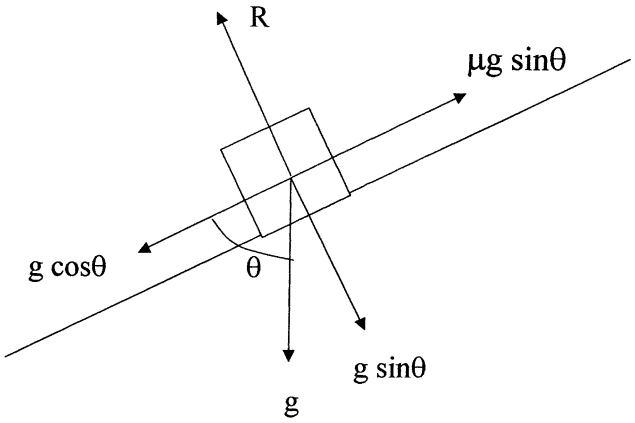

Figure 3. Force balance on a fluid element for determination of tortuosity effect.

can be read as the tortuosity factor τ. Correlating the trend on pressure drop and holdup with experimental data set available in the literature, the following model equations have been suggested for the dependence of tortuosity on the superficial liquid and gas velocities

$$\tau = \cos \theta - \mu \sin \theta. \quad (17)$$

In an earlier approach (Tung and Dhir, 1988), the particle–gas drag was modified with the flow regime transitions to account for tortuosity. As in the present approach, the depiction of the tortuosity effect takes care of the flow regime transitions, so redefinition of particle–gas drag with the flow regime transition is not required. Thus, under the new model, flow regimes would not play any role in determining the particle–gas drag.

It is now important to determine θ and μ as functions of the gas and liquid velocities. It is observed that as the gas and

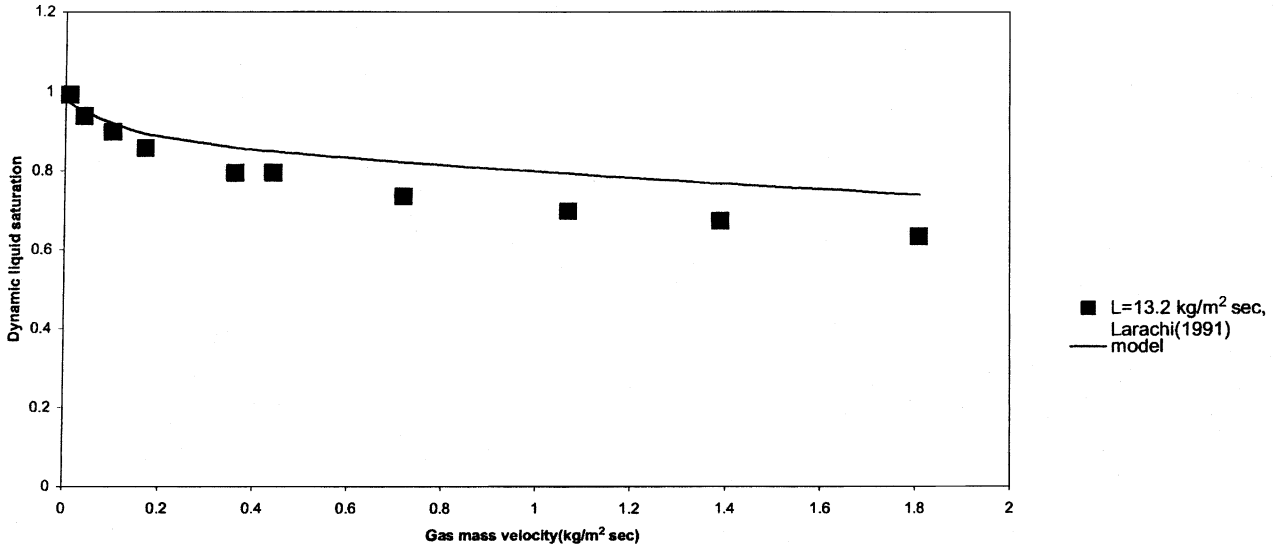

Figure 4. Dynamic liquid saturation vs. superficial gas mass velocity.

Comparison of the theoretical predictions with the experimental results of Larachi et al. (1991a). (L = 13.2 kg/m^2·s, P = 2.1 MPa).

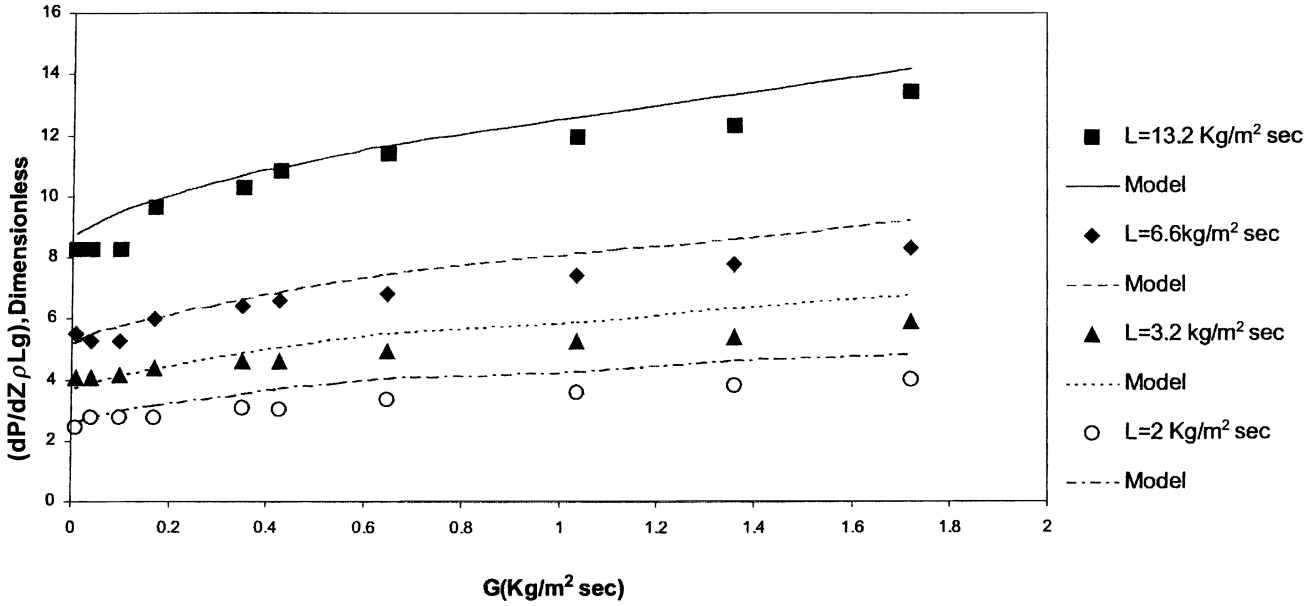

Figure 5. Dimensionless pressure gradient vs. superficial gas mass velocity.

Comparison of the theoretical predictions with the experimental results of Larachi et al. (1991a). (Ethylene glycol-nitrogen, $P = 5.1$ MPa.)

liquid velocities increase, the tortuosity also increases and follows the following relations

$$d\theta/dV_1 \propto (\pi/2 - \theta), \tag{18}$$

where $V_1 = V_L + V_G$. In other words, the relative change in tortuosity with velocity is proportional to the difference between maximum tortuosity and the existing tortuosity.

The preceding relationship yields

$$\theta = \frac{\pi}{2}\{1 - e^{-K(V_L + V_G)}\}, \tag{19}$$

where K (a constant) depends on the physical properties of the fluids.

The friction factor (μ) reduces with the increase in velocity, as this has the effect of aiding the motion. The relation-

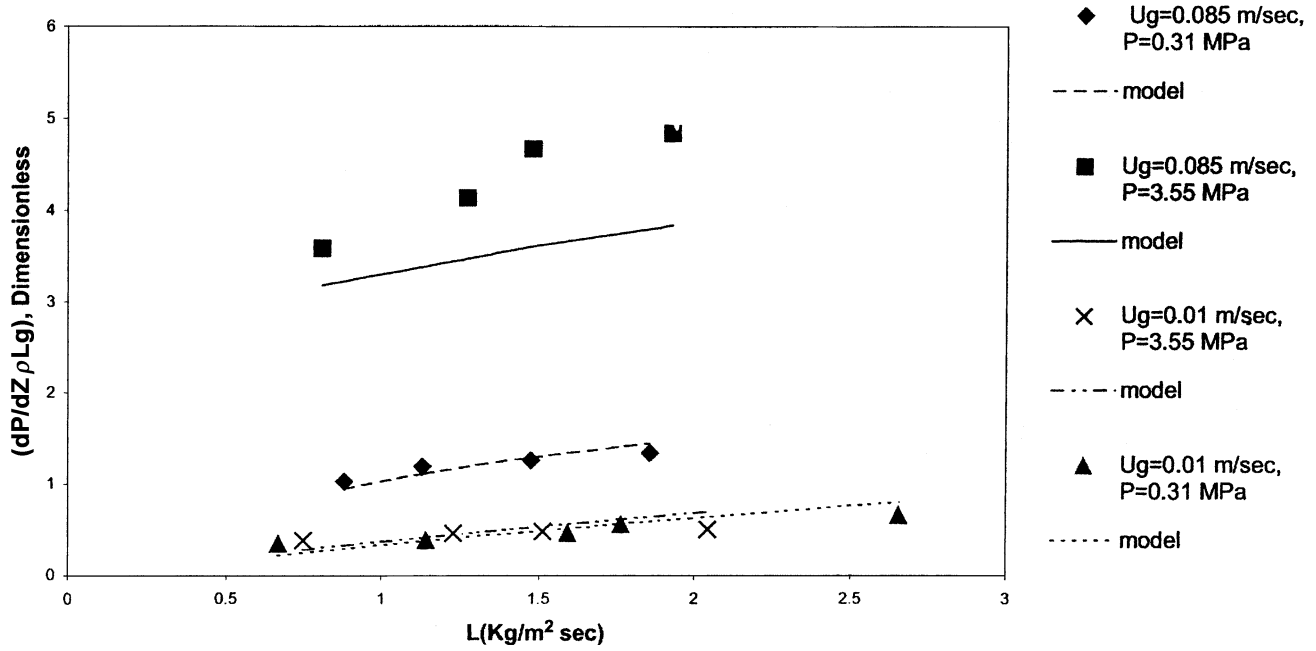

Figure 6. Dimensionless pressure gradient vs. superficial liquid mass velocity.

Comparison of predictions of model with the data of Al-Dahhan and Dudukovic (1994). (Porous silica shell, hexane-nitrogen.)

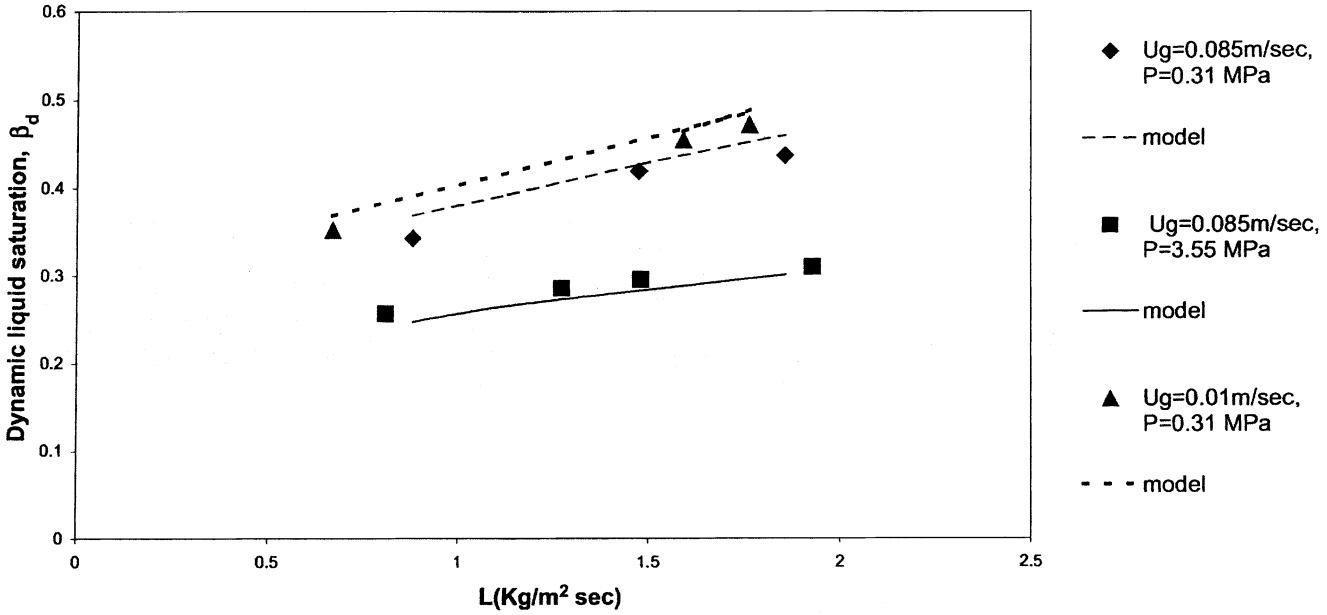

Figure 7. Dynamic liquid saturation vs. superficial liquid mass velocity.

Theoretical predictions vs. experimental results of Al-Dahhan and Dudukovic (1994). Porous silica shell, hexane-nitrogen.

ship can be expressed as

$$d\mu/dV = 1/V_1^N, \tag{20}$$

which translates to

$$\mu = k_1 - k_2(N-1)/V_1^{N-1}, \tag{21}$$

where k_1 and k_2 are constants whose values depend on the system under discussion. It also found that $N = 2$ provides a good estimate for the phenomenon.

For the present air–water system, Eq. 21 reduces to the following

$$\mu = k_1 - k_2/(V_L + V_G). \tag{22}$$

The axial dispersion effect has been considered in a novel method in which back-mixing has been found to play a crucial role. Due to back-mixing, the liquid is found to travel

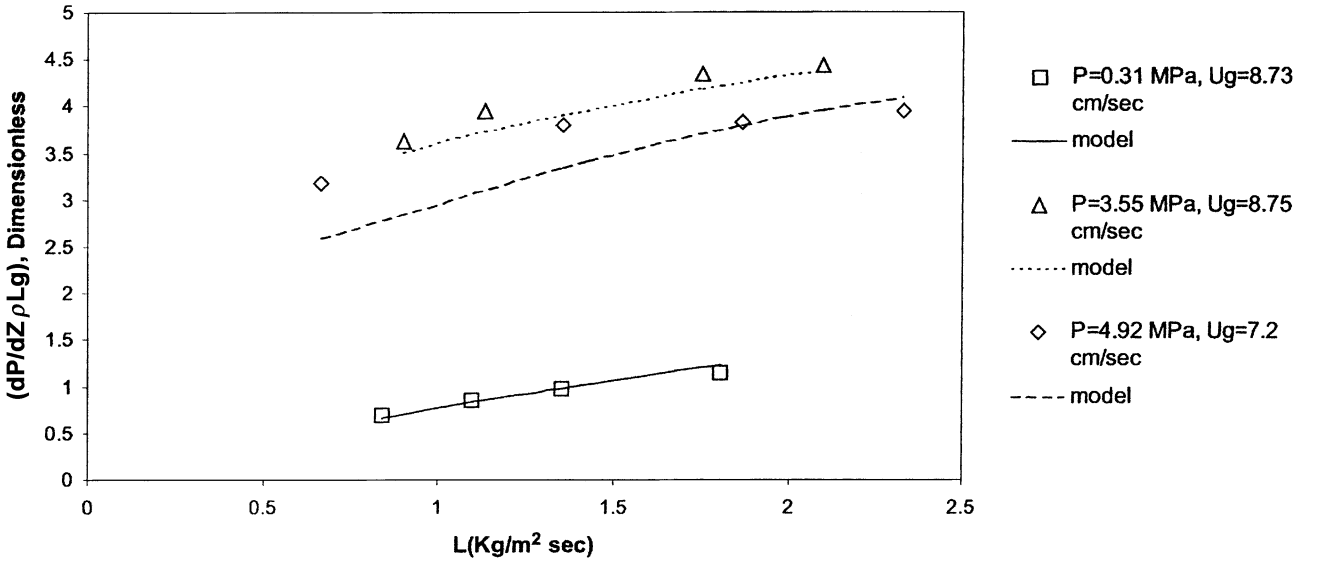

Figure 8. Dimensionless pressure gradient vs. superficial liquid mass velocity.

Theoretical predictions vs. experimental results of Al-Dahhan and Dudukovic (1994). Porous extrudate of 0.5% Pd on alumina, hexane-nitrogen.

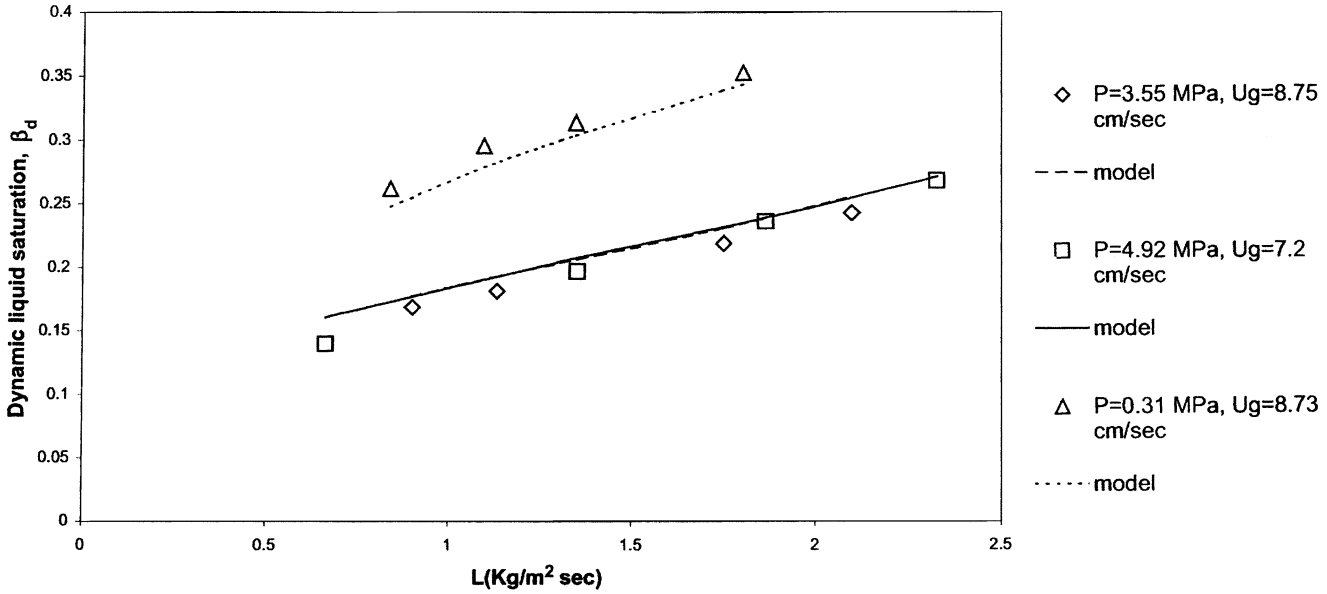

Figure 9. Dynamic liquid saturation vs. superficial liquid mass velocity.

Theoretical predictions vs. experimental results of Al-Dahhan and Dudukovic (1994). Porous extrudates of 0.5% Pd on alumina, hexane-nitrogen.

farther and the mean residence time increases, as given by the following equation

$$\theta_m = \mathrm{tc}/T = 1 + 2D/V_L L_1 = 1 + 2/Pe_L. \qquad (23)$$

Thus it is assumed that there will be a distribution of length traveled by the fluid particles corresponding to the time taken by it to travel the reactor. Hence a theoretical length, L'_1 is considered, which is given by

$$L'_1 = L_1(1 + 2/Pe_L). \qquad (24)$$

Due to the extra length caused by back-mixing diffusion, swirls, and so on, the pressure drop increases for a given reactor length, which is considered in the model. The pressure drop is corrected using the preceding factor for the extra

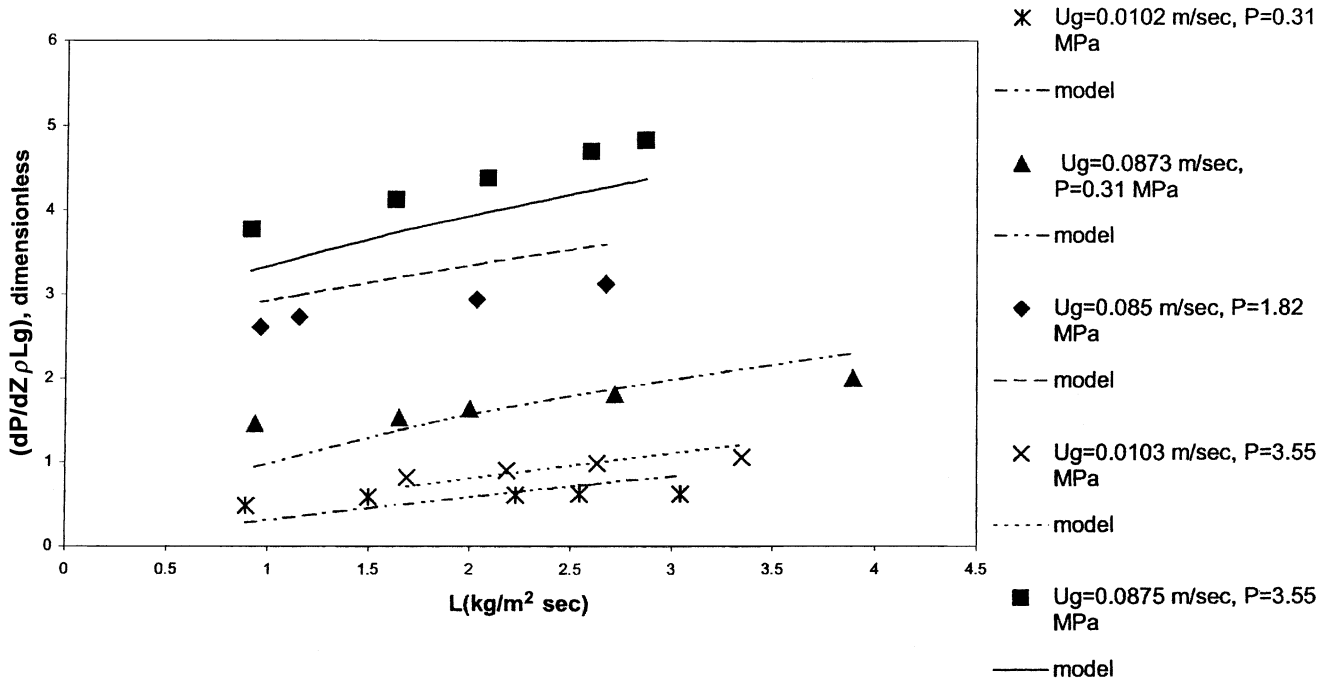

Figure 10. Dimensionless pressure gradient vs. superficial liquid mass velocity.

Theoretical predictions vs. experimental results of Al-Dahhan and Dudukovic (1994). Porous extrudates of 0.5% Pd on alumina, water–nitrogen.

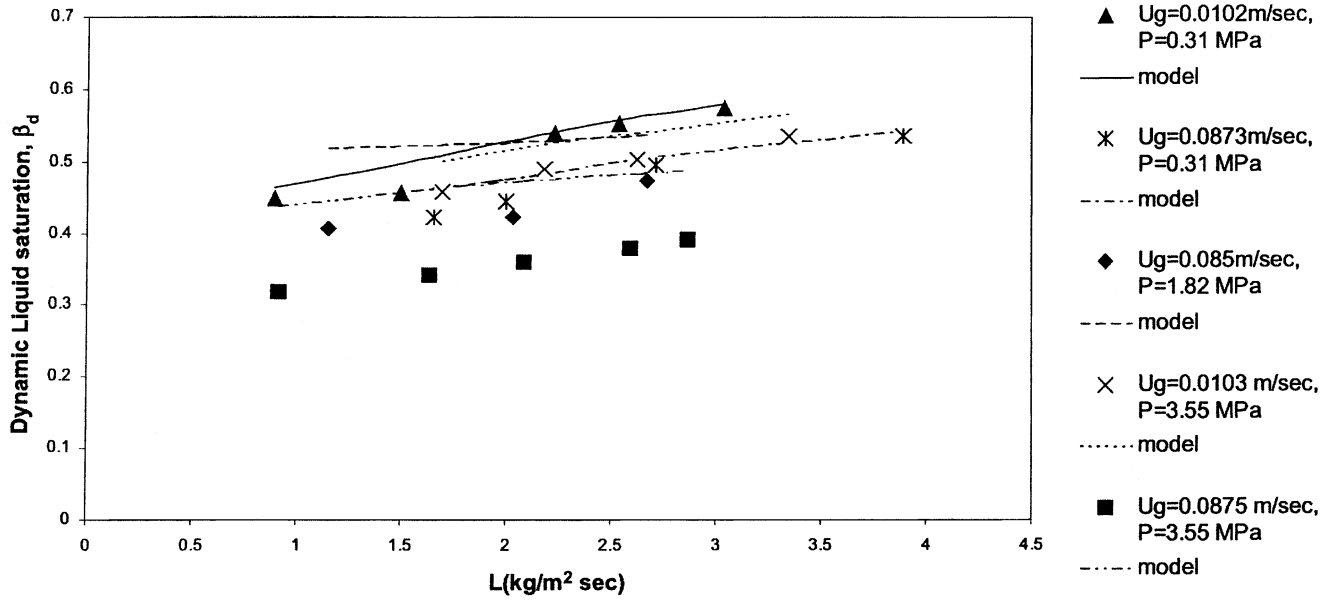

Figure 11. Dynamic liquid saturation vs. liquid mass velocity.

Theoretical predictions vs. experimental results of Al-Dahhan and Dudukovic (1994). Porous extrudates of 0.5% Pd on alumina, water–nitrogen.

length actually traversed by the fluid element due to the axial dispersion effect within a given unit length of the reactor bed.

In the expressions for tortuosity just given, μ, which denotes the frictional losses, is high at low velocities. This is in agreement with the observation of Mears (1971). In addition, θ, which accounts for the extra distance traveled by the phases, should increase with the superficial velocities. Indeed both these observations are implemented by the preceding model.

Combination of the Models. The models for particle–gas drag, particle–liquid drag, and the liquid–gas interfacial drag are now used in conjunction with the force balances on the liquid and gas phases to predict the liquid saturation and the pressure drop. Elimination of the pressure gradient between the two dimensionless force balance equations (Eqs. 7 and 8) yields the following nonlinear equation

$$\alpha(1-\alpha)\tau + F_{PG}^{*}(1-\alpha) - \alpha F_{PL}^{*} + F_{I}^{*} = 0. \qquad (25)$$

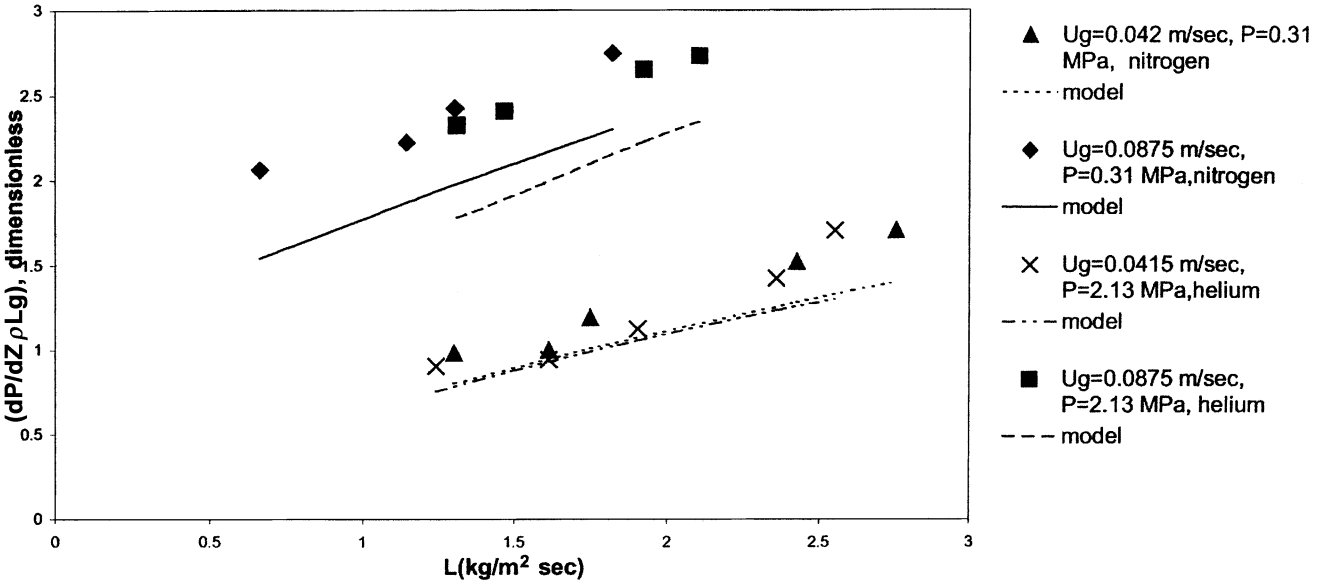

Figure 12. Dimensionless pressure gradient vs. superficial liquid mass velocity.

Theoretical predictions vs. experimental results of Al-Dahhan and Dudukovic (1994). Porous extrudates of 0.5% Pd on alumina, water–nitrogen, and helium.

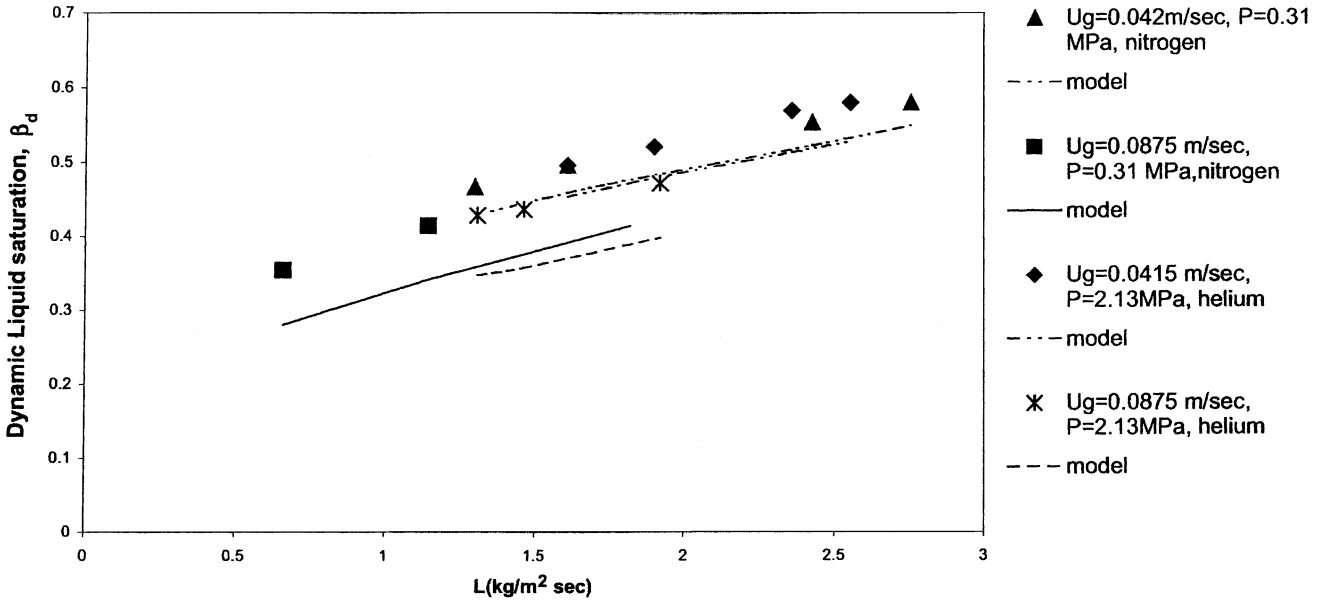

Figure 13. Dynamic liquid saturation vs. superficial liquid mass velocity.

Theoretical predictions vs. experimental results of Al-Dahhan and Dudukovic (1994). Porous extrudates of 0.5% Pd on alumina, water–nitrogen, and helium.

For the given superficial velocities, V_L and V_G, determination of the gas saturation α is accomplished by solving the preceding equation by using the Newton–Raphson algorithm with successive substitution.

Once the value of α is obtained by this procedure, the liquid saturation can be obtained as $\beta = 1 - \alpha$, and the pressure drop can be calculated by solving Eq. 7 or Eq. 8.

The dynamic liquid saturation is calculated from the present model by the relation $\beta_d = 1 - \alpha - \beta_s$, where the static liquid saturation, β_s, has been determined experimentally by the authors. Wherever the authors have not reported the static liquid saturation, the correlation of Wammes et al. (1991) has been recommended.

Results

Larachi et al. (1991a,b) have presented pressure-gradient and dynamic liquid-saturation measurements for concurrent

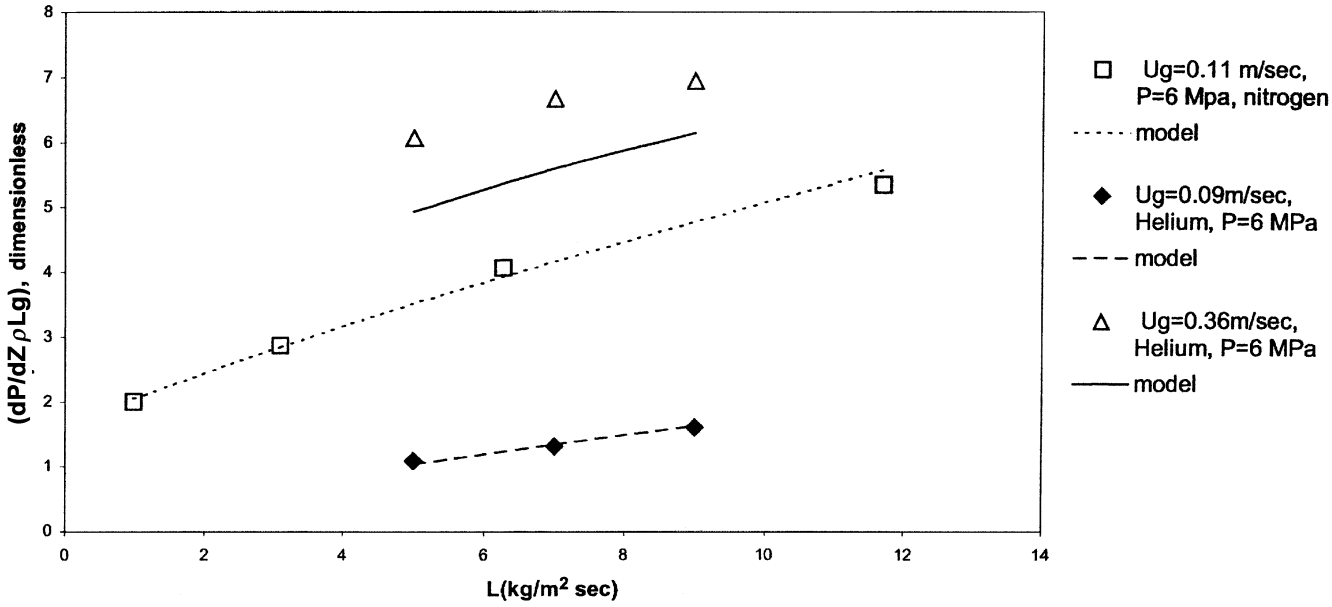

Figure 14. Dimensionless pressure gradient vs. superficial liquid mass velocity.

Theoretical predictions vs. experimental results of Wammes et al. (1991a,b). Nonporous glass beads, water–nitrogen, and helium.

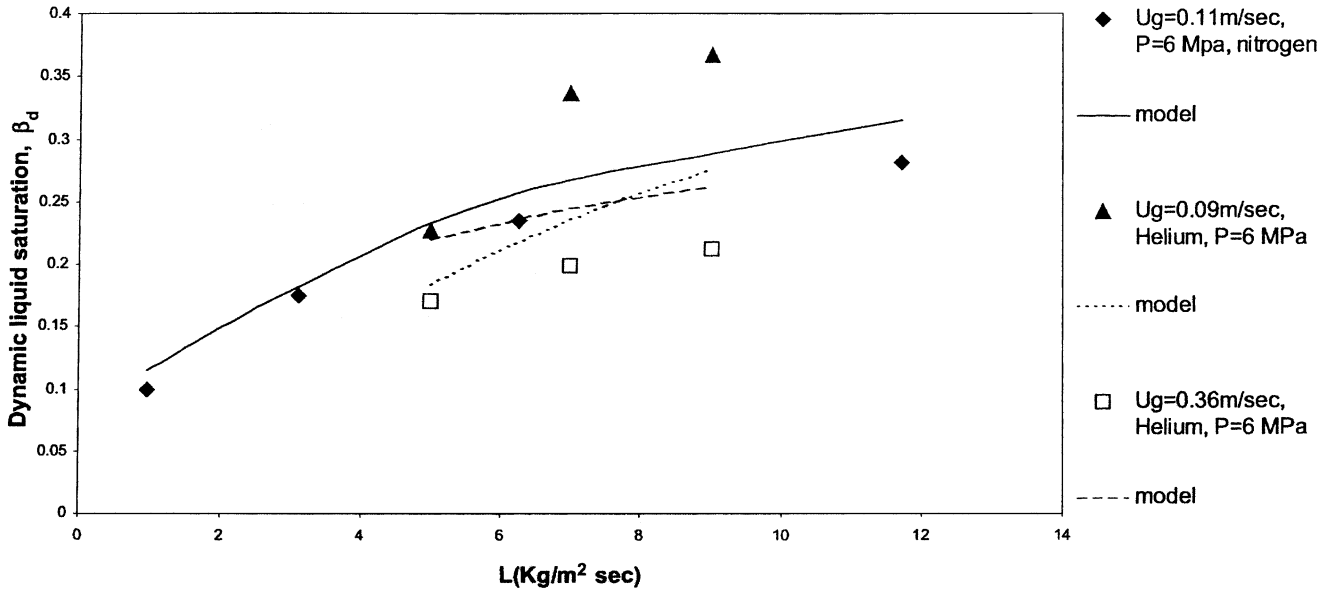

Figure 15. Dynamic liquid saturation vs. superficial liquid mass velocity.

Theoretical predictions vs. experimental results of Wammes et al. (1991a,b). Glass beads, water–nitrogen, and helium; $P = 6$ MPa.

gas–liquid downward flows through packed beds of glass beads in the operating pressure range 0.2–8.1 MPa. The model predictions have been compared with the experimental results of Larachi et al. (1991a) for liquid holdup and pressure gradient in Figures 4 and 5, respectively. The theoretical model is able to predict quite well the significant influence of the gas flow rate on the hydrodynamic parameters.

Al-Dahhan and Dudokovic (1994) have performed pressure-gradient and total liquid-saturation measurements for cocurrent gas–liquid trickle flow through packed beds of glass beads, porous spherical silica, and porous extrudate in the operating pressure range of 0.31–5 MPa. The theoretical predictions from the model are compared with the experimental results of Al-Dahhan and Dudukovic in Figures 6, 8, 10 and 12 for pressure gradient, and Figures 7, 9, 11 and 13 for liquid saturation.

Wammes and Westerterp (1991) and Wammes et al. (1991a, b) have performed pressure-gradient and dynamic liquid-

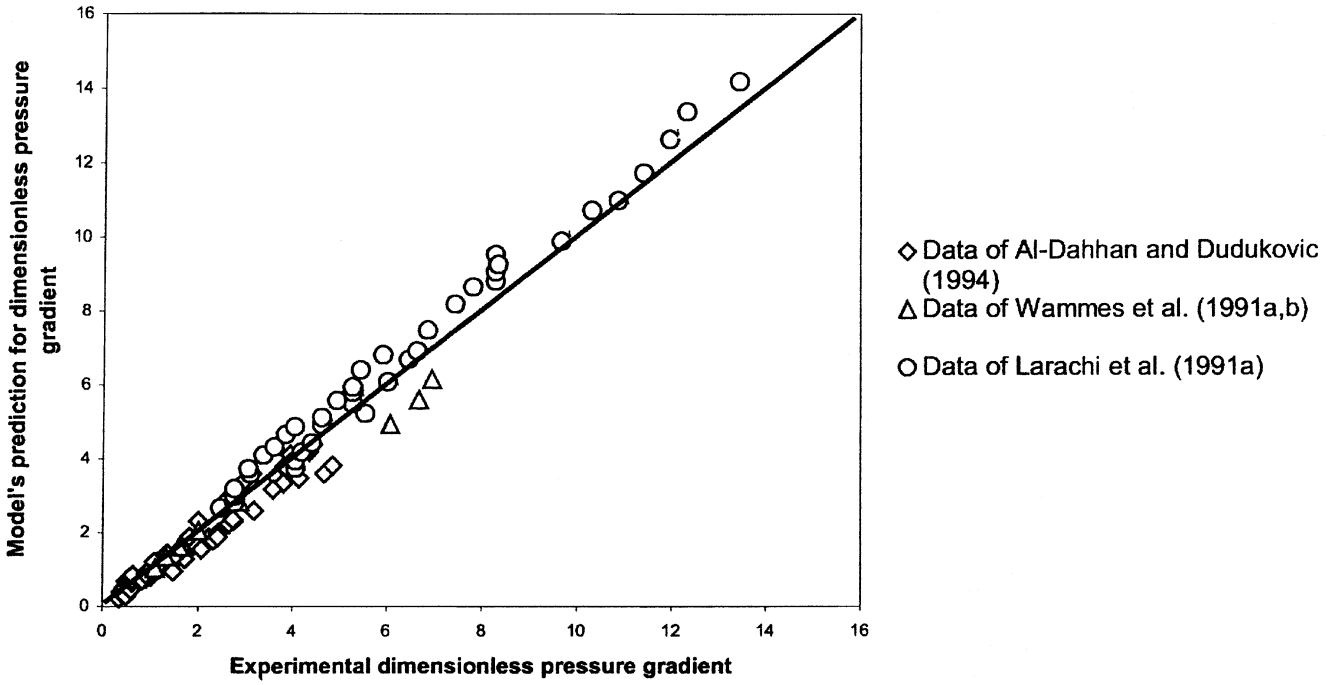

Figure 16. Parity plot of pressure gradient for the experimental data sets.

Larachi et al., 1991a; Wammes et al., 1991a,b; Al-Dahhan and Dudukovic, 1994.

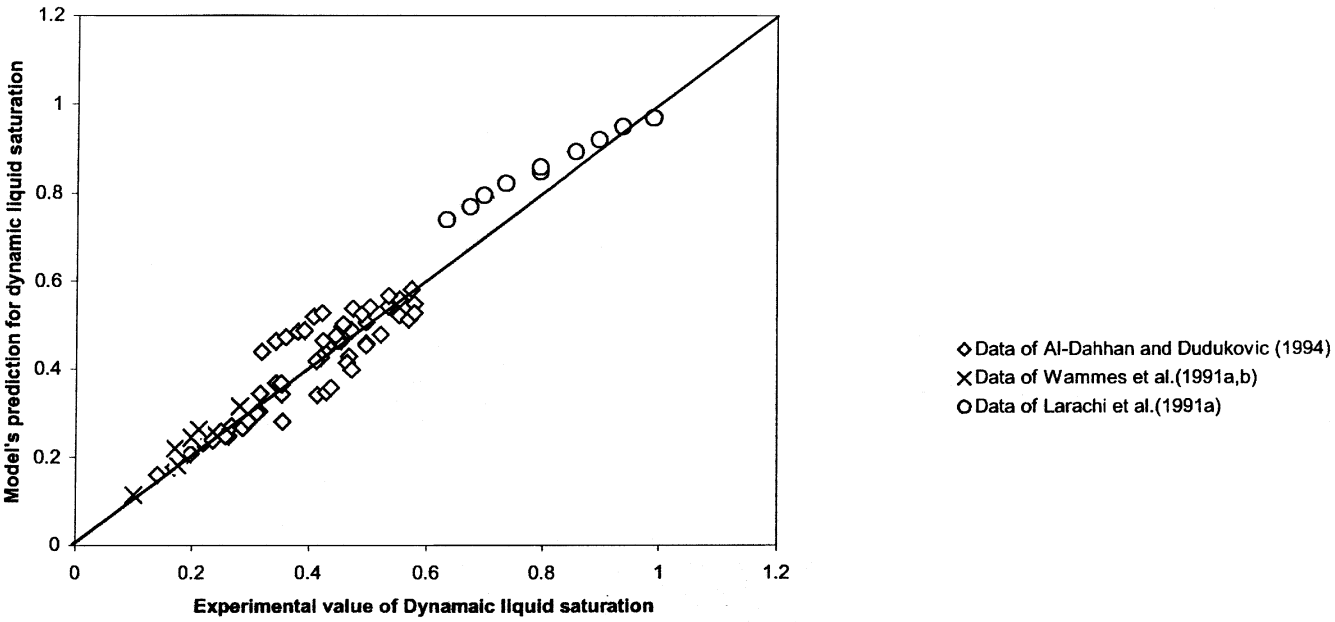

Figure 17. Parity plot of dynamic liquid saturation for the experimental data sets.

Larachi et al., 1991a; Wammes et al., 1991a,b; Al-Dahhan and Dudukovic, 1994.

saturation measurements for cocurrent gas–liquid trickle flow through packed beds of glass beads and ceramic cylinders in the pressure range of 0.2–7.5 MPa. At an operating-pressure value equal to 6 MPa and with two different gases (helium and nitrogen), the predictions of the model are compared with experimental results in Figures 14 and 15 for pressure gradient and dynamic liquid saturation, respectively. Figures 16 and 17 show the parity plot for all the experimental data of the pressure drop and dynamic liquid saturation, respectively, used for verifying the model.

It also has been found that the model can be applied to foaming liquids or coalescence inhibiting liquids. Charts com-

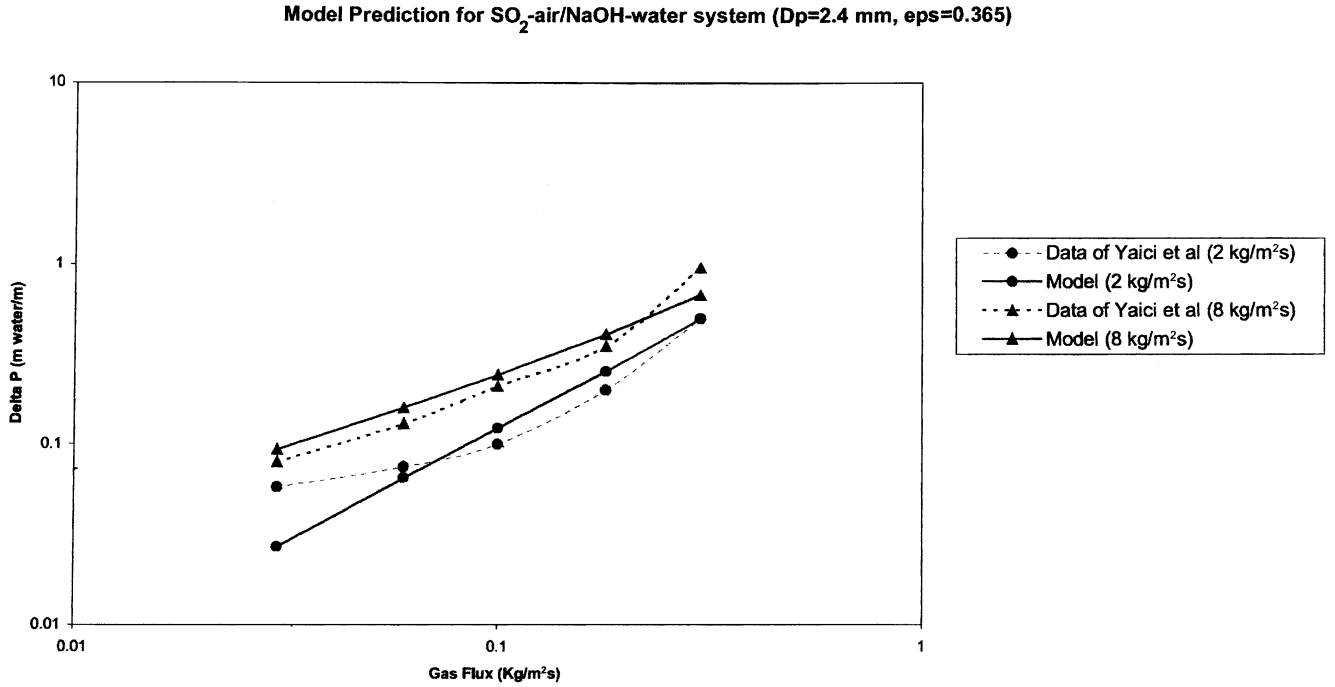

Figure 18. Pressure gradient vs. superficial gas mass velocity.

Theoretical predictions vs. experimental results of Yaici et al. (1988). $NaOH/SO_2$–air, $D_P = 0.0024$ m, $\epsilon = 0.365$, $L = 2$ kg/m^2·s, and 8 kg/m^2·s).

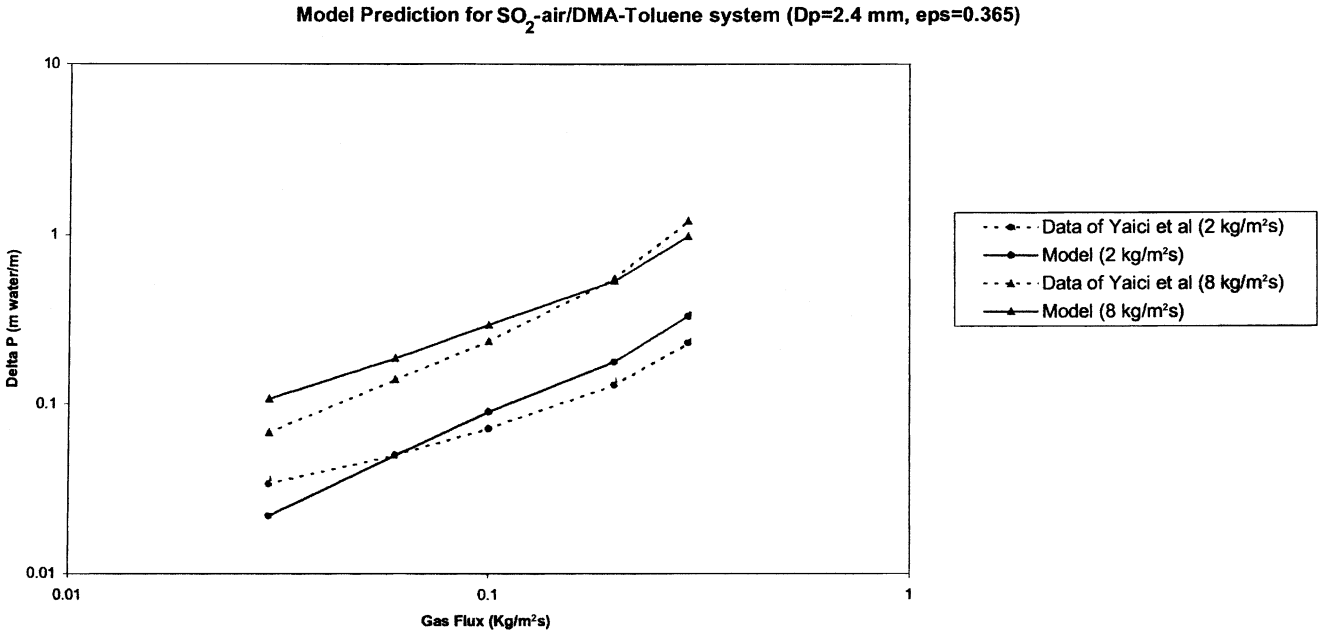

Figure 19. Pressure gradient vs. superficial gas mass velocity.

Theoretical predictions vs. experimental results of Yaici et al. (1988). DMA–toluene/SO_2–air, $D_P = 0.0024$ m, $\epsilon = 0.365$, $L = 2$ kg/m^2·s, and 8 kg/m^2·s.

paring model predictions with experimental data on pressure drop for the SO_2–air/DMA–toluene system (Yaici et al., 1988) and the SO_2–air/NaOH system (Yaici et al., 1988) are shown in Figures 18 and 19. Charts comparing pressure-gradient predictions for the propyl carbonate–helium system (Larachi et al., 1991a) is shown in Figure 20, and the aqueous MDEA/antifoam–carbon dioxide system (Wammes et al., 1991) is shown in Figure 21. Figure 22 shows a comparison between the dynamic saturation prediction for the propylene carbonate-nitrogen system (Larachi et al., 1991a). The prediction accuracy in all of these cases has been found within the accuracy level of the model shown in Table 1.

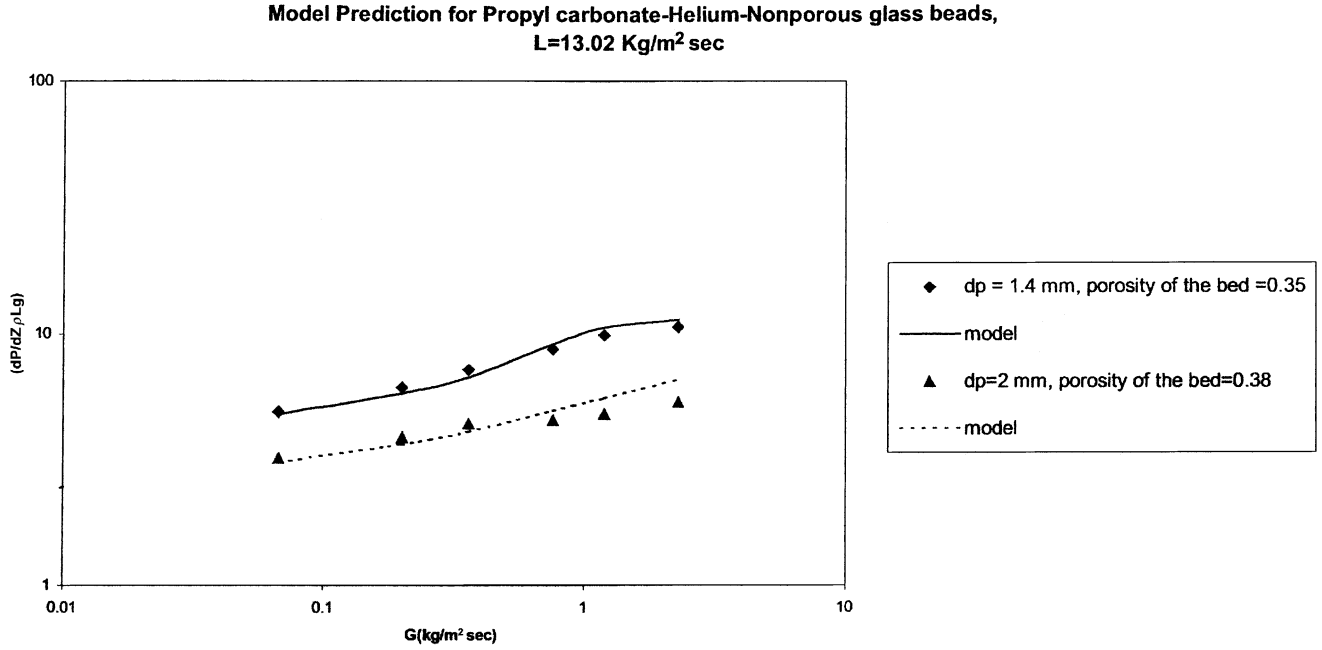

Figure 20. Dimensionless pressure gradient vs. superficial gas mass velocity.

Theoretical predictions vs. experimental results of Larachi et al. (1991a). Nonporous glass beads, propylene carbonate–helium, $L = 13.2$ kg/m^2·s, and $P = 2.1$ MPa.

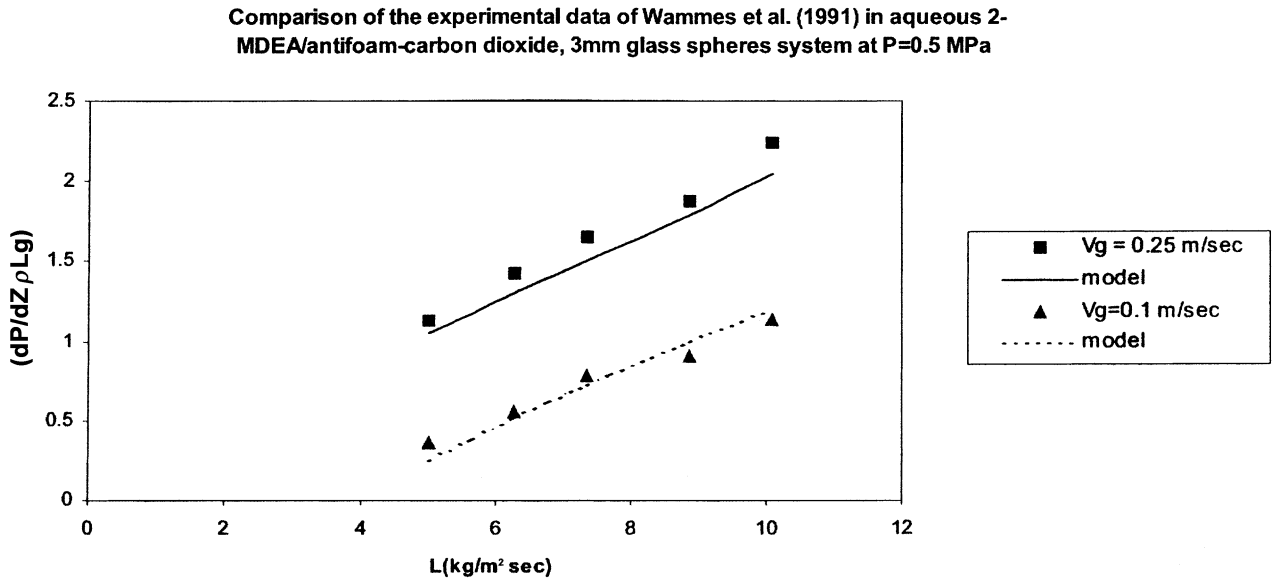

Figure 21. Dimensionless pressure gradient vs. superficial liquid mass velocity.

Theoretical predictions vs. experimental results of Wammes et al. (1991b). Glass sphere, aqueous 2-MDEA–antifoam/CO_2, $P = 0.5$ MPa.

Comparison of predictions from the model and available correlations with experimental data

The mean relative error $\langle e_\psi \rangle$ between the predicted and experimental values of the hydrodynamic parameter ψ (pressure gradient or liquid saturation) is calculated from

$$\langle e_\psi \rangle = \frac{1}{N} \sum_{1}^{N} \frac{|\psi_{\text{predicted}} - \psi_{\text{experimental}}|}{\psi_{\text{experimental}}}. \qquad (26)$$

The results of mean relative errors obtained by comparing the theoretical results of each correlation and model with the experimental data sets of Wammes et al. (1991), Larachi et al. (1991a,b), and Al-Dahhan and Dudukovic (1994) are, respectively, presented in Table 1. This table demonstrates the virtuosity of the current model. The reason for significant improvement in the proposed approach might be (as opposed to the available correlations) that the present model is based on a formulation deduced from fundamental macroscopic balance laws, as well as a more realistic description of the physics of various interaction phenomena in trickle-bed reactor. Iliuta et al. (2000) predicts somewhat better than other previous models, but their predictions were found to be less accurate at higher superficial gas velocity. Although the value of

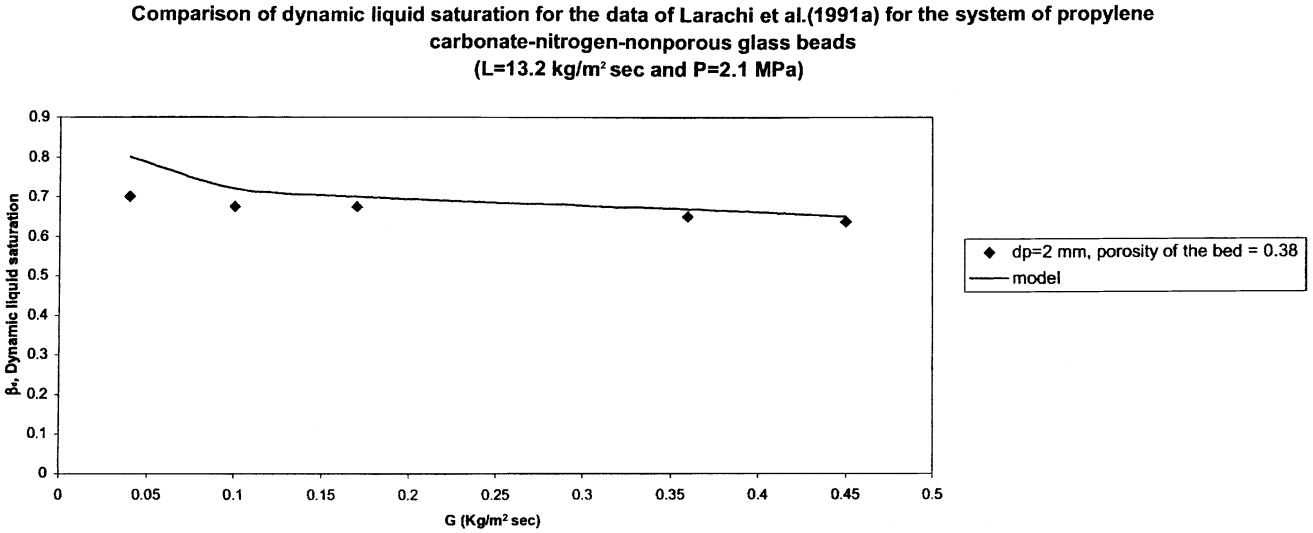

Figure 22. Dynamic liquid saturation vs. superficial gas mass velocity.

Theoretical predictions vs. experimental results of Larachi et al. (1991a). Nonporous glass beads, propylene carbonate–nitrogen, $L = 13.2$ kg/m^2·s, and $P = 2.1$ MPa.

Table 1. Model's Prediction vs. Experimental Data in Terms of Statistical Parameter $\langle e_\psi \rangle$

Mean Rel. Error	Wammes et al.	Ellman et al.	Larachi et al.	Holub et al.	Iliuta et al.	Present Model
Pres. gradient	0.524	0.648	0.766	0.530	0.370	0.187
Liquid saturation	0.230	0.334	0.272	0.132	0.150	0.125

the mean relative error of pressure drop and liquid holdup is similar to that observed by Larachi et al. (2000), the values of the mean relative error of pressure drop reported in Larachi et al. (2000) from different models are on the high side compared to Table 1. This is due to the prediction of pressure drop and liquid holdup from the correlation approach in Larachi et al. (2000).

Discussion and Conclusion

A unique physics-based model has been proposed for modeling trickle-bed reactors at elevated pressures for predicting the hydrodynamics (pressure drop and liquid holdup). The unified approach includes fundamental point force balance and takes tortuosity effects into account. The tortuosity effect is included in the force balance in terms of gravity. This factor takes the extra energy losses (and, hence, pressure drop) into account. It has also been found that the tortuosity effects are gas and liquid velocity dependent, with the effect of gas velocity being prominent at high superficial gas mass velocities.

The theoretical predictions from the model correctly account for the strong influence of the gas flow on the hydrodynamic behavior of the trickle-bed reactors, as shown by the various pertinent experiments examined in this work. The important influence of the gas flow is attributed to the interactions phenomena exerted by the gas phase on the liquid phase. These interactions clearly appear to be significant at high superficial gas mass velocities.

The novel hydrodynamic model has been found to predict some proprietary data satisfactorily, but the authors are unable to report them, because they are bound by a data secrecy agreement.

It was found that the model predicts with a reasonable accuracy the experimental data, which comprises a variety of systems, including hydrocarbon, foaming liquids, and coalescence-inhibiting liquids (Wammes et al., 1991a,b; Larachi et al., 1991a,b; Al-Dahhan and Dudukovic, 1994; Yaici et al., 1988). The trickle flow regime is usually described as low gas-liquid interaction. Strictly speaking, weak interfacial gas–liquid interaction prevails only at very low superficial gas and liquid velocities. However, as the superficial gas velocities are increased toward the pulsing regime, the interaction between the gas and liquid is enhanced, especially with increasing pressure. Thus, the interfacial gas–liquid interaction greatly influences the prediction of the macroscopic hydrodynamic variables, namely, the total pressure drop and the liquid holdup.

Notation

a = constant, $[150(1-\epsilon)^2]/(\epsilon^3 D_P^2)$
a^* = constant, $a/[g(\rho_L - \rho_G)]$
b = constant, $[1.75(1-\epsilon)]/(\epsilon^3 D_P)$
b^* = constant, $b/[g(\rho_L - \rho_G)]$
C'_I = inertial drag coefficient
C'_V = viscous drag coefficient
D_P = particle diameter or equivalent particle diameter, m
D_b = bubble diameter, m
D = eddy diffusion coefficient, m^2/s
e = mean relative error
E_1, E_2 = Ergun constant for the single-phase flow on the packing
F^* = dimensionless drag force, $F/[g\epsilon(\rho_L - \rho_G)]$
F_I = liquid–gas interfacial drag, $kg \cdot m^{-2} \cdot s^{-2}$
F_I^* = dimensionless liquid–gas interfacial drag, $F_I/[g\epsilon(\rho_L - \rho_G)]$
F_{PG} = particle–gas drag, $kg \cdot m^{-2} \cdot s^{-2}$
F_{PG}^* = dimensionless particle-gas drag, $F_{PG}/[(g\epsilon(\rho_L - \rho_G)]$
F_{PL} = particle–liquid drag, $kg \cdot m^{-2} \cdot s^{-2}$
F_{PL}^* = dimensionless particle–liquid drag, $F_{PL}/[g\epsilon(\rho_L - \rho_G)]$
g = gravitational acceleration, m/s^2
G = superficial gas mass velocity, $kg \cdot m^{-2} \cdot s^{-1}$
h_L = liquid holdup
L = superficial liquid mass velocity, $kg \cdot m^{-2} \cdot s^{-1}$
L_1 = catalyst bed length, m
L'_1 = actual distance traveled by the liquid, m
P^* = dimensionless pressure gradient, $(dP/dZ)/[g(\rho_L - \rho_G)]$
Pe = Peclet number, $L_1/(DV)$
Re = Reynolds number defined as $(Q/A\epsilon)(\rho/\mu)Dp[\epsilon/(1-\epsilon)]$.
T = mean residence time in the whole reactor, s
t_c = elapsed time, s
V_s = drift velocity of bubble relative to the mixture, $m \cdot s^{-1}$, $[V_G(1-\alpha)/\alpha] - V_L$
V = superficial velocity, m/s

Greek letters

α = gas saturation
β = liquid saturation
γ = ratio of bubble diameter to equivalent particle diameter
η = ratio of average distance between two adjacent particles to equivalent particle diameter
ϵ = porosity of packed bed
θ = inclination angle, rad
θ_m = mean of the dimensionless residence time distribution
σ = surface tension, $kg \cdot s^{-2}$
τ = tortuosity factor
μ = model friction factor
μ_G = viscosity of the gas phase, $kg/m \cdot s$
μ_L = viscosity of the liquid phase, $kg/m \cdot s$
ρ_G = density of the gas phase, $kg \cdot m^{-3}$
ρ_L = density of the liquid phase, $kg \cdot m^{-3}$
ν_L = kinematic viscosity of liquid, $m^2 \cdot s^{-1}$
ρ^* = dimensionless density, $\rho^* = \rho_L/\rho_G$
κ_G, η_G = gas relative permeabilities
κ_L, η_L = liquid relative permeabilities
ψ = hydrodynamic parameter

Subscripts

L = liquid phase
G = gas phase
I = gas–liquid interface
t = total
d = dynamic
s = static

Literature Cited

Al-Dahhan, M. H., and M. P. Dudukovic, "Pressure Drop and Liquid Holdup in High-Pressure Trickle Bed Reactors," *Chem. Eng. Sci.*, **49**, 5681 (1994).

Al-Dahhan, M. H., M. R. Khadilkar, Y. Wu, and M. P. Dudukovic, "Prediction of Pressure Drop and Liquid Holdup in High-Pressure Trickle-Bed Reactors," *Ind. Eng. Chem. Res.*, **37**, 793 (1998).

Al-Dahhan, M. H., and W. Highfill, "Liquid Holdup Measurement Techniques in Laboratory High Pressure Trickle Bed Reactors," *Can. J. Chem. Eng.*, **77**, 759 (1999).

Attou, A., C. Boyer, and G. Ferschneider, "Modelling of the Hydro-

dynamics of the Cocurrent Gas-Liquid Trickle Flow Through a Trickle-Bed Reactor," *Chem. Eng. Sci.*, **54**, 785 (1999).
Charpentier, J. C., C. Prost, and P. Le Goff, "Pressure Drop in Trickle Flow Compared to Bubble Flow for Two Phase Flow in Cocurrent Gas-Liquid in Packed Beds," *Chem. Eng. Sci.*, **24**, 1777 (1969).
Charpentier, J. C., and M. Favier, "Some Liquid Holdup Experimental Data in Trickle Bed Reactors for Foaming and Non-foaming Hydrocarbons," *AIChE J.*, **21**, 1213 (1975).
Clements, L. D., and P. C. Schmidt, "Two Phase Pressure Drop in Cocurrent Downflow in Packed Beds: Air-Silicone Oil Systems," *AIChE J.*, **26**, 314 (1980).
Ellman, M. J., N. Midoux, A. Laurent, and J. C. Charpentier, "A New Improved Pressure Drop Correlation for Trickle-Bed Reactors," *Chem. Eng. Sci.*, **43**, 2201 (1988).
Ellman, M. J., N. Midoux, G. Wild, A. Laurent, and J. C. Charpentier, "A New Improved Liquid Holdup Correlation for Trickle Bed Reactors," *Chem. Eng. Sci.*, **45**, 1677 (1990).
Ergun, S., "Fluid Flow Through Packed Columns," *Chem. Eng. Prog.*, **48**, 89 (1952).
Gianetto, A., V. Specchia, and G. Baldi, "Absorption in Packed Towers with Cocurrent Downward High Velocity Flows, *Part II: Mass transfer*," *AIChE J.*, **19**, 916 (1973).
Hasseni, W., A. Laurent, N. Midoux, and J. C. Charpentier, "Hydrodynamics of a Trickle Bed Reactor Operating Under Pressure (0–10 MPa): Flow Regimes and Pressure Drop," *CHISA' 87*, Session 17: Gas-Liquid Packed Bed, Prague (1987).
Holub, R. A., M. P. Dudukovic, and P. A. Ramachandran, "A Phenomenological Model for Pressure Drop, Liquid Holdup, and Flow Regime Transition in Gas-Liquid Trickle Flow," *Chem. Eng. Sci.*, **47**, 2343 (1992).
Holub, R. A., M. P. Dudukovic, and P. A. Ramachandran, "Pressure Drop, Liquid Holdup, and Flow Regime Transition in Trickle Flow," *AIChE J.*, **39**, 302 (1993).
Iliuta, I., A. Ortiz-Arroyo, F. Larachi, B. P. A. Grandjean, and G. Wild, "Hydrodynamics and Mass Transfer in Trickle-Bed Reactors: An Overview," *Chem. Eng. Sci.*, **54**, 5329 (1999).
Iliuta, I., F. Larachi, and M. H. Al-Dahhan, "Double-Slit Model for Partially Wetted Trickle Flow Hydrodynamics," *AIChE J.*, **46**, 597 (2000).
Kundu, A., A. K. Saroha, and K. D. P. Nigam, "Liquid Distribution Studies in Trickle-Bed Reactors," *Chem. Eng. Sci.*, **56**, 5963 (2001).
Larachi, F., A. Laurent, N. Midoux, and G. Wild, "Experimental Study of a Trickle Bed Reactor Operating at High Pressure: Two-Phase Pressure Drop and Liquid Saturation," *Chem. Eng. Sci.*, **46**, 1233 (1991a).
Larachi, F., A. Laurent, N. Midoux, and G. Wild, "Some Experimental Liquid Saturation Results in Fixed-Bed Reactors Operated Under Elevated Pressure in Cocurrent Upflow and Downflow of the Gas and the Liquid," *Ind. Eng. Chem. Res.*, **30**, 2404 (1991b).
Larachi, F., I. Iliuta, M. A. Al-Dahhan, and M. P. Dudukovic, "Discriminating Trickle-Flow Hydrodynamic Models: Some Recommendations," *Ind. Eng. Chem. Res.*, **39**, 554 (2000).
Larkins, R. P., R. R. White, and D. W. Jeffery, "Two-Phase Co-Current Flow in Packed Beds," *AIChE J.*, **7**, 231 (1961).
McCabe, W. L., J. C. Smith, and P. Harriot, *Unit Operations of Chemical Engineering*, 5th ed., McGraw-Hill, Singapore (1993).
Mears, D. E., "Test for Transport Limitation in Experimental Catalytic Reactors," *Ind. Eng. Chem. Process Des. Dev.*, **10**, 541 (1971).
Midoux, N., M. Favier, and J. C. Charpentier, "Flow Pattern, Pressure Loss and Liquid Holdup Data in Gas-Liquid Down-Flow Packed Beds with Foaming and Non-Foaming Hydrocarbons," *J. Chem. Eng. Jpn.*, **9**, 305 (1976).
Nigam, K. D. P., A. K. Saroha, A. Kundu, and H. J. Pant, "Radioisotope Tracer Study in Trickle Bed Reactors," *Can. J. Chem. Eng.* (2001).
Pant, H. J., A. Kundu, and K. D. P. Nigam, "Radiotracer Applications in Chemical Process Industry," *Rev. Chem. Eng.*, **17**, 165 (2001).
Rao, V. G., and A. A. H. Drinkenburg, "A Model for Pressure Drop in Two-Phase Gas-Liquid Downflow through Packed Columns," *AIChE J.*, **31**, 1010 (1985).
Sáez, A. E., and R. G. Carbonell, "Hydrodynamic Parameters for Gas-Liquid Cocurrent Flow in Packed Beds," *AIChE J.*, **31**, 52 (1985).
Sai, P. S. T., and Y. B. G. Varma, "Pressure Drop in Gas-Liquid Downward Flow Through Packed Beds," *AIChE J.*, **33**, 2027 (1987).
Saroha, A. K., and K. D. P. Nigam, "Trickle Bed Reactor," *Rev. Chem. Eng.*, **12**, 207 (1996).
Sato, Y., T. Hirose, F. Takahashi, and M. Toda, "Pressure Loss and Liquid Holdup in Packed Bed Reactor with Co-Current Gas-Liquid Down-Flow," *J. Chem. Eng. Jpn.*, **6**, 147 (1973).
Specchia, V., and G. Baldi, "Pressure Drop and Liquid Holdup for Two-Phase Concurrent Flow in Packed Beds," *Chem. Eng. Sci.*, **32**, 515 (1977).
Sweeney, D. E., "A Correlation for Pressure Drop in Two-Phase Concurrent Flow in Packed Beds," *AIChE J.*, **13**, 663 (1967).
Tosun, G., "Study of Co-Current Down-Flow of Non-Foaming Gas-Liquid Systems in a Packed Bed: I. Flow Regime: Search for a Generalized Flow Map; 2. Pressure Drop: Search for a Correlation," *Ind. Eng. Chem. Process Des. Dev.*, **23**, 29 (1984).
Tung, V. X., and V. K. Dhir, "A Hydrodynamic Model for Two Phase Flow Through Porous Media," *Int. J. Multiphase Flow*, **14**, 47 (1988).
Turpin, J. L., and R. L. Hungtinton, "Prediction of Pressure Drop for Two-Phase, Two Component Co-Current Flow in Packed Beds," *AIChE J.*, **6**, 1196 (1967).
Wammes, W. J. A., and K. R. Westerterp, "Hydrodynamics in a Pressurized Cocurrent Gas-Liquid Trickle-Bed Reactor," *Chem. Eng. Technol.*, **14**, 406 (1991).
Wammes, W. J. A., S. J. Mechielsen, and K. R. Westerterp, "The Influence of Pressure on the Liquid Hold-Up in a Cocurrent Gas-Liquid Trickle-Bed Reactor Operating at Low Gas Velocities," *Chem. Eng. Sci.*, **46**, 409 (1991a).
Wammes, W. J. A., J. Middelkamp, W. J. Huisman, C. M. deBaas, and K. R. Westerterp, "Hydrodynamics in a Cocurrent Gas-Liquid Trickle Bed at Elevated Pressures," *AIChE J.*, **37**, 1849 (1991b).
Xiao, Q., A. M. Anter, Z. M. Cheng, and W. K. Yuan, "Correlations for Dynamic Liquid Holdup Under Pulsing Flow in a Trickle-Bed Reactor," *Chem. Eng. J.*, **78**, 125 (2000).
Yaici, W., A. Zaurent, N. Midoux, and J. C. Charpentier, "Determination of Gas Side Mass Transfer Co-Efficient in Trickle Bed Reactors in Presence of an Aqueous or an Organic Liquid Phase," *Int. Chem. Eng.*, **28**, 299 (1988).

Manuscript received Jan. 30, 2001, and revision received Feb. 14, 2002.